HHS Public Access

Author manuscript

J Biophotonics. Author manuscript; available in PMC 2020 May 01.

Published in final edited form as:

J Biophotonics. 2019 May ; 12(5): e201800307. doi:10.1002/jbio.201800307.

In vivo detection of endotracheal tube biofilms in intubated critical care patients using catheter-based optical coherence tomography

Roshan Dsouza[1], **Darold R. Spillman Jr.**[1], **Ronit Barkalifa**[1], **Guillermo L. Monroy**[1,2], **Eric J. Chaney**[1], **Karen C. White**[3], and **Stephen A. Boppart**[1,2,4,5,*]

[1]Beckman Institute for Advanced Science and Technology, University of Illinois at Urbana-Champaign, 405 N Mathews Ave, Urbana, Illinois 61801, USA

[2]Department of Bioengineering, University of Illinois at Urbana-Champaign, 1270 Digital Computer Laboratory, MC-278, Urbana, Illinois 61801, USA

[3]Critical Care Medicine, Carle Foundation Hospital, 611 W. Park Street, Urbana, Illinois 61801, USA

[4]Carle-Illinois College of Medicine, University of Illinois at Urbana-Champaign, 807 S. Wright St., Urbana, Illinois 61801, USA

[5]Department of Electrical and Computer Engineering, University of Illinois at Urbana-Champaign, 306 N. Wright St., Urbana, Illinois 61801, USA

Abstract

The formation of biofilms in the endotracheal tubes (ETTs) of intubated patients on mechanical ventilation is associated with a greater risk of ventilator-associated pneumonia (VAP) and death. New technologies are needed to detect and monitor ETTs *in vivo* for the presence of these biofilms. Longitudinal OCT imaging was performed in mechanically ventilated subjects at 24 hr intervals until extubation to detect the formation and temporal changes of *in vivo* ETT biofilms. OCT-derived attenuation coefficient images were used to differentiate between mucus and biofilm. Extubated ETTs were examined with optical and electron microscopy, and all imaging results were correlated with standard-of-care clinical test reports. OCT and attenuation coefficient images from 4 subjects were positive for ETT biofilms and were negative for 2 subjects. The processed and stained extubated ETTs and clinical reports confirmed the presence/absence of biofilms in all

*Corresponding Author: boppart@illinois.edu.

Conflict of Interest

S.A. Boppart is co-founder and Chief Medical Officer of PhotoniCare, Inc., which is developing optical imaging systems for the ear, and Diagnostic Photonics, Inc., which is developing optical imaging systems for cancer detection. S.A.B. also reports intellectual property owned by the Massachusetts Institute of Technology and the University of Illinois at Urbana-Champaign related to optical coherence tomography, and licensed to commercial entities. The remaining authors have disclosed that they do not have any conflicts of interest.

Ethics approval and consent to participate

This observational study was approved by the Institutional Review Boards of Carle Foundation Hospital and the University of Illinois at Urbana-Champaign (reference 16CRU1498). Written informed consent was obtained from the patient's legal guardians, and any patient data was de-identified before it was provided to researchers.

Supporting Information

Additional supporting information may be found in the online version of this article at the publisher's website.

subjects. Our findings confirm that OCT can detect and differentiate between biofilm-positive and biofilm-negative groups ($p < 10^{-5}$). OCT image-based features may serve as biomarkers for direct *in vivo* detection of ETT biofilms and help drive investigation of new management strategies to reduce the incidence of VAP.

Graphical Abstract

Longitudinal *in vivo* catheter-based 3-D OCT imaging of endotracheal tubes in mechanically ventilated critical care patients was performed to detect and monitor resident biofilms. The acquired OCT volumes and calculated attenuation coefficients were correlated with conventional microscopy and clinical reports. Results demonstrated the potential for OCT to not only detect and monitor the formation of biofilms, but also differentiate biofilms from mucus. OCT image-based features may serve as new biomarkers for the investigation of management strategies to reduce the incidence of ventilator-associate pneumonia and death.

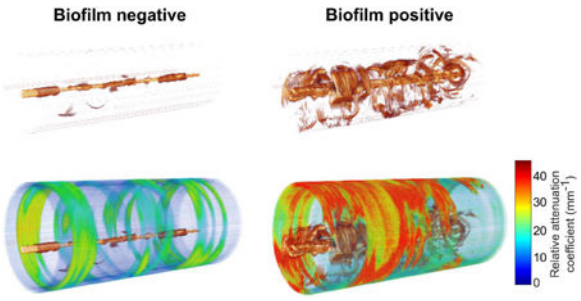

Keywords

biofilm; endotracheal tube; ventilator-associated pneumonia; optical coherence tomography; attenuation coefficient image

1. Introduction

Precise and prompt monitoring in intensive care medicine is crucial for the management of patients with life threatening conditions, often necessitating either organ/life support and/or invasive monitoring. Under critical conditions, patients are supported by mechanical ventilation with an endotracheal tube (ETT) to facilitate pulmonary gas exchange and relieve breathing distress. However, this intervention increases the risk of nosocomial infections that can lead to ventilator-associated pneumonia (VAP) and death [1–5]. Of the 1.6 million patients in the US who require some form of mechanical ventilation each year, 15–25% develop VAP, and 24–71% will die [6–8]. Mortality in patients with lung infections and/or on mechanical ventilators is 24% for patients 15–19 years old and 60% for patients older than 85 years [9].

VAP in critical care patients is reported to develop within 48 h post-intubation [10]. The warm, moist, and humid environment within an *in vivo* ETT promotes the growth and survival of various pathogenic bacteria which often develop bacterial biofilms [11]. Biofilms are complex microbial communities that secrete an extracellular polysaccharide matrix, enabling survival, protection, proliferation, and an increasingly drug-resistant bacterial population[12]. The

structure of a biofilm is intricate, which facilitates exchange of fluids, nutrients, and waste products amidst the bacterial cells, which in turn enables proliferation and dispersion of a bacterial load to new locations. Bacterial biofilms are widely observed on and within medical devices such as cardiac pacemakers[13], prosthetic heart valves[14], intravenous and urinary catheters[14, 15], contact lenses[16], and ETTs[17]. The microstructure of biofilms is inherently three-dimensional (3-D), eventually producing planktonic bacteria that attach to a surface and initially form thin films. The bacteria continue to proliferate and form thicker biofilms which then further disseminate throughout the area or region, such as the respiratory tract, establishing new growth areas[18].

VAP is conventionally diagnosed using radiological techniques (planar X-ray and computed tomography), ultrasound imaging, microbiological techniques, non-quantitative or semi-quantitative airway sampling, and quantitative cultures of airway specimens [19–23]. However, none of these tests can accurately identify *in vivo* biofilm formation at the point-of-care. Development of a non-invasive real-time diagnostic technique enabling the detection and development of an ETT biofilm in intubated patients offers the potential for improved management strategies for these critical patients.

OCT is the optical analogue to ultrasound imaging, which detects light reflections rather than sound, and performs cross-sectional label-free imaging in real-time with high-resolution. Contrast in OCT images is based on variations in optical index of refraction and the density of scatterers. In other studies, our group has demonstrated the presence of *in vivo* biofilms in the middle ear using OCT, in agreement with biological characterization [24–26]. Furthermore, OCT has successfully been used to detect biofilms in extubated ETTs [27] and in intubated neonates for laryngotracheal wall imaging [28]. In the previous study [27], OCT imaging was performed on extubated (*ex vivo*) ETTs following a 40-min transport time, and analysis was done based on only film thickness measurements. This previous study did not incorporate a method to differentiate the presence of mucus or biofilm, or a combination of both, nor was the effect of the suctioning procedure evaluated on OCT analysis. Importantly, this study did not investigate the *in vivo* development and longitudinal growth of ETT biofilms, which is key information for making clinical decisions.

This study reports *in vivo* monitoring and optical characterization of ETT biofilm formation in 6 critical care patients using catheter-based 3-D OCT. Longitudinal OCT imaging was performed in intubated subjects every 24-hours until extubation. Extubated ETTs were subsequently analyzed with scanning electron microscopy (SEM) and fluorescence and Gram staining. OCT and attenuation coefficient image analysis results were correlated with microscopy and clinical data to verify the presence of bacteria and biofilm. Pixel-wise attenuation coefficient image analysis enabled differentiation between mucus and biofilm. The clinical translation of this technology could enable new patient management strategies to effectively reduce the incidence of VAP in critical care patients.

2. Methods and Materials

2.1. Study population

This observational study was conducted with a cohort of six subjects (irrespective of ethnicity, gender, or race) under critical care. Subjects included in this study were admitted to the intensive care unit (ICU) of Carle Foundation Hospital, Urbana, IL, USA, and required mechanical ventilation for over 24 h. Informed consent was obtained from the subject's guardian / relative in accordance with protocols approved by the Institutional Review Boards of Carle Foundation Hospital and the University of Illinois at Urbana-Champaign.

2.2 Longitudinal OCT imaging and extubated ETT collection

Radial (cylindrical) 3-D OCT imaging was performed *in vivo* within the lumens of ETTs in intubated patients using a commercial catheter-based OCT system (Model C7XR, St. Jude Medical, Inc.). The OCT system had an axial scan rate of 50 kHz, enabling high-speed radial imaging over a pullback distance of 5.4 cm in 5 s. Each OCT catheter (Dragonfly model C7, St. Jude Medical, Inc.) was 1.35 m in length, with an outer diameter of 0.9 mm. The OCT system and catheter optics provided a 20 μm axial and 45 μm transverse resolution (depending on radial distance from the catheter), and an imaging depth range of 4.83 mm. Figure 1 illustrates *in vivo* OCT imaging of an ETT. The catheter fiber- and micro-optics rotate 360^0 within a stationary transparent outer sheath to form a radial cross-sectional image of the ETT and cylindrical volumetric data is obtained by scanning in a spiral scanning pattern during pullback. Each radial image within the volume depicts the inner and outer surface of the ETT along with any biofilm and/or mucus formation on the inner surface. The inner diameter of the adult-sized ETT was approximately 8.5 mm and the imaging depth-of-field of the catheter system and the working distance were approximately 4.6 mm and 5 mm, respectively. Due to the larger diameter adult-sized ETT and this limited depth-of-field, we were not able to capture the entire circumference of the inner ETT lumen in an OCT image, as it was not possible to center the catheter within the ETT during imaging. Hence, during imaging, the catheter was located along the inner surface of the ETT and the attenuation coefficient image corresponded to an average of 100 pixels extending radially outward from the outer sheath of the catheter. The acquired images were within the depth-of-field of the system.

At the start of each longitudinal imaging period, a physician inserted a new sterile OCT catheter through the suctioning/bronchoscopy access port and into the ETT. The research team controlled the acquisition of the OCT system. The OCT catheter was previously marked to indicate the total length and distal end of the ETT, ensuring positioning of the catheter within the ETT lumen and not extending into the trachea. The length of the catheter allowed for imaging of the entire ETT, which comprised 5 cylindrical volumes (pull-backs). Following acquisition of the cylindrical 3-D OCT datasets (total imaging time < 10 min), the catheter was withdrawn from the ETT and disinfected (Revital-Ox Resert, 4455-AW) for 8 min after each use. The catheter was then stored in a sterile bag for subsequent imaging of the same subject. Imaging was performed at 24-hour intervals until extubation, which was dictated by standard-of-care patient management. A new sterile OCT imaging catheter was

used for each new subject, and disinfected after each use per the above protocol. Extubated ETTs were transported to the laboratory (5 min travel time) and fixed in fixative solution (2.0% paraformaldehyde and 2.5% glutaraldehyde in 0.1 M Na-Cacodylate buffer) until further analysis.

2.3 OCT image analysis

The 3-D cylindrical volume reconstruction of each OCT dataset consisted of 976 × 504 × 269 (rows, columns, and radial scans along pull-back) pixels, respectively, which were processed and saved in *tiff* format. A pixel-wise attenuation coefficient algorithm [29] was processed for each radial OCT image in the volume. Attenuation coefficients represent the rate of optical signal decay due to absorption and scattering of light from the sample, facilitating differentiation between mucus and biofilm due to their different optical scattering properties. The slick and aqueous texture of mucus renders it largely translucent to light [30]. Unlike mucus, biofilm is comprised of a more highly-scattering extracellular matrix, along with a large population of scattering bacterial cells that form a protective barrier and a stable, adherent texture [31]. The attenuation coefficient $\boldsymbol{\mu}[\mathbf{i}]$ was estimated from the OCT intensity images, divided by the total number of pixels along an A-scan $N(976)$, and the pixel size Δ in millimeters by:

$$\boldsymbol{\mu}[\mathbf{i}] = \frac{I[i]}{2\Delta\sum_{\mathbf{i}+1}^{N} I[i]} . \quad (1)$$

The relative attenuation coefficient (RAC) was obtained by applying the structural mask to the attenuation coefficient $\boldsymbol{\mu}[\mathbf{i}]$ to reduce the background noise. The RAC image is displayed circumferentially around the radial OCT image and corresponds to an average of 100 pixels extending radially outward from the outer surface of the catheter as shown in Figure 1C. The mean RAC was calculated by measuring the mean attenuation throughout the entire length of the ETT (5 OCT volumes corresponding to 27 cm in ETT length).

2.4 Microscopy of endotracheal tube content

The extubated and fixed ETTs were cut longitudinally and opened to expose the inner luminal surface of the ETT and any adherent biological material (biofilm and/or mucus). Samples of this material were suspended in saline and then centrifuged to recover the supernatant that was subsequently smeared on glass microscope slides. These prepared samples were processed for Gram staining. These samples were also embedded in paraffin and subsequently processed for fluorescent staining using a Biofilm Cell stain (FilmTracer FM 1–43, Invitrogen) and a Biofilm Matrix Stain (FilmTracer SYPRO Ruby, Invitrogen), according to the manufacturer's instructions, and observed under a fluorescence microscope (Axiovert 200, Zeiss). Samples were also processed and imaged with scanning electron microscopy (FEG 450, FEI Quanta) at 10,000 keV with a magnification of 10,000× and 13,000×.

2.5 Statistical analysis

The statistical analysis of the measurements between the biofilm-negative and biofilm-positive groups was done using a two-tailed Welch's *t* test. A significance level of $p < 0.05$ was considered statistically significant. The statistical calculation was implemented in Matlab using the *ttest2* function. Data variables were expressed as mean ± standard deviation.

3 Results

The acquired OCT and RAC images were processed for each subject. The RAC images were analyzed based on the hypothesis that biofilm has higher attenuation/scattering, compared to mucus, due to the presence of the extracellular matrix and many scattering bacteria. Longitudinal OCT and RAC images were used to differentiate between biofilm-positive and biofilm-negative ETTs (Figure 2). Representative longitudinal radial OCT scans of a subject (Subject 6, Table 1) showed formation of a structure on the inner luminal surface of the ETT (Figure 2, top row) while the subject was intubated for 3 days. However, these OCT images show scattering structures accompanied by air bubbles. A lower RAC extracted from these radial scans plausibly corresponded to the presence of mucus. Similarly, longitudinal OCT images from Subject 2 (Table 1) were acquired for 6 days. Representative OCT and RAC images for Subject 2 are shown in Figure 2 (bottom row). The scattering and thickness of the structures in the OCT images were comparable to images shown in the top row. However, RAC images of the biofilm-positive ETT (Subject 2) showed increased attenuation, in contrast to the biofilm-negative ETT (Subject 6).

The reconstructed 3-D cylindrical volumes of the OCT and RAC images are shown in Figure 3. The volume for the biofilm-positive ETT (Subject 2, Day 6) shows the presence and random distribution of the biofilm throughout the ETT, in contrast to the biofilm-negative ETT (Subject 6, Day 3). The RAC value was calculated from the 3-D volume data after considering the mean attenuation throughout the volume.

A quantitative analysis of RAC for the ETTs from all the subjects is summarized in Figure 4. Figure 4A shows the mean RAC for 6 subjects (Table 1) from the day of intubation until extubation. The attenuation profiles for the biofilm-negative ETTs (green) showed a trend of decreasing attenuation over the days of intubation. However, the attenuation profiles of the biofilm-positive ETTs showed a higher degree of optical attenuation (red) over the intubation period. Figure 4B shows a histogram plot and fit of RAC values for the biofilm-positive and biofilm-negative groups. The analysis shown in Figure 4B was done by averaging the attenuation coefficient values from all of the radial scans, and then statistically analyzing for differences between biofilm positive and negative groups. The RAC distribution for the biofilm-negative ETTs ranged between 5 - 25 mm^{-1}, in contrast to 5 - 55 mm^{-1} for biofilm-positive ETT's. Despite the demarcation between the groups, lower RAC values in the biofilm-positive ETTs may be due to the non-uniform spatial distribution of biofilm (along with the presence of mucus) throughout the ETT. This could be deduced by considering the volume for biofilm imaged within the ETT (Figure 3D (Subject 2, Day 6)), where the radial scans within the volume showed lower attenuation, and could be due to mucus alone. This is likely the case for the varied RAC and the bimodal distribution (Figure

S1 and S2) throughout all of the biofilm-positive ETTs. Each distribution (1st and 2nd) can be separated by fitting a Gaussian mixture model. The mean and standard deviation of the biofilm-negative group was 14.9 ± 6.6 mm^{-1}, while the biofilm-positive group (1st distribution) and biofilm-positive group (2nd distribution) are shown in Figure 4C. The statistical analysis shows that RAC metrics can differentiate biofilm-negative ETTs from biofilm-positive ETTs, 2nd distribution ($p < 10^{-5}$).

To substantiate and validate the presence or absence of biofilm and correlate with OCT and RAC images, extubated ETTs were fixed, processed, and imaged using conventional microscopic techniques. All extubated ETTs were processed for Gram staining and fluorescence staining for biofilm, and SEM. We selected OCT images from the last day of imaging, and biomaterial samples (biofilm and/or mucous) from approximately from the same region were obtained for Gram, biofilm, and SEM analysis. The recovered biomaterial samples from the extubated ETTs were therefore approximately co-registered with the corresponding OCT images. Figure 5 shows representative microscopic images from ETTs that were positive (Subject 2) and negative (Subject 6) for biofilm. Gram staining of a biofilm-positive ETT showed clusters of bacteria (Gram positive rods) embedded in a complex matrix, in contrast to a biofilm-negative ETT, corroborating an earlier report [32]. Structure of the biofilm under SEM was compared with known morphology [33]. Similarly, SEM images of the biofilm-positive ETT showed extracellular matrix with embedded bacteria, in contrast to a biofilm-negative ETT. Furthermore, fluorescence staining for the biofilm cells and matrix corroborated with the other microscopy techniques for differentiating the presence or absence of a biofilm. The microscopy data validated the findings from the catheter-OCT system.

OCT findings and microscopy data were further correlated to the clinical reports. Table 1 summarizes the clinical records of each subject from Day 1 of intubation until extubation. As demonstrated by OCT and microscopic image data, Subject 2 was clinically reported to have developed pneumonia on the sixth day of intubation. The RAC images of the biofilm-positive ETT (Subject 2) showed the presence of a biofilm from Day 3-6. Whereas RAC images of Subject 6 showed a biofilm-negative ETT, consistent with clinical reports. The OCT and RAC image-based data from all the subjects included in the study were consistent with microscopic and clinical findings. Thus, these results suggest that the OCT-based attenuation coefficient images can detect and track *in vivo* biofilm formation in intubated patients.

4 Discussion

Formation of biofilms in the ETTs of ventilated patients plays a direct role in the development of VAP [33]. Given the unmet need for real-time point-of-care detection and monitoring of ETT biofilms in ventilated patients, imaging by catheter-based OCT provides a non-invasive (no more invasive than intubation of an ETT) means to identify these biofilms. Importantly, this new technology and methodology will enable new research and clinical investigations into the etiology of ETT biofilm formation, their response to interventions such as suctioning and antibiotics, and further correlations between the onset and development of ETT biofilms and the occurrence of VAP. In the future, catheter-based

3D OCT could provide new insights and data for critical care physicians to ensure effective suctioning and brush cleaning procedures of an ETT. If suctioning or cleaning fails to remove an adherent biofilm, OCT image data would be used to justify replacing a bacteria-colonized ETT with a new ETT in order to reduce the risk of VAP. The replacement of a bacterial biofilm-infected ETT would be analogous to the practice of replacing various arterial and venous catheters and lines with new ones in the setting of a patient with a systemic infection.

Typically, development of VAP in ventilated patients is assessed by a radiological imaging (chest X-ray) and diagnosed by microbial culture [19, 20, 23]. Although, a chest X-ray can indicate pneumonia, it does not determine the presence of an ETT biofilm, which is thought to be a primary risk factor for VAP. In contrast, our study reports a feasible real-time, minimally-invasive, bedside imaging technique for detecting and monitoring the development of an ETT biofilm. Statistical analysis showed significant differences in RAC metrics between the biofilm-negative and biofilm-positive groups ($p < 10^{-5}$). In one representative subject (Subject 2), our investigation demonstrated the presence and development of a biofilm from Day 3-6 with increased attenuation longitudinally over time. The clinical reports indicated that the subject was diagnosed with pneumonia on Day 6, which may represent a causal relationship that needs to be supported further with a larger clinical study. Currently, conventional microbiological diagnostics require laborious sample preparation procedures and require time for a conclusive diagnosis. Current procedures also do not permit real-time monitoring, and require repeated sampling with an inherent delay in feedback to the critical care physician for medical decision making. Implemented as a point-of-care imaging modality, catheter-based OCT distinctly enables longitudinal *in vivo* monitoring for ETT biofilms, which may help reduce the associated risks of VAP and death.

Novel treatment regimens and methods for targeting and eradicating ETT biofilms are an active area of research, including nebulized (aerosol) gentamicin [34], lock therapy [35], non-thermal plasma treatments [36], and photodynamic therapy [37]. Nonetheless, an efficacious therapy demands a robust and efficient detection or monitoring technique, particularly for early-stage investigations of these potential treatments and other interventions. Unlike conventional techniques, our system distinctly enables longitudinal *in vivo* monitoring of ETT biofilms. Earlier investigations have reported the detection of ETT biofilms post-extubation [32, 33, 38]. One study demonstrated the presence of biofilm in an extubated ETT using OCT images, where the images were acquired 40 min post-extubation [27]. However, from our study, we found that interpreting structural OCT images (biological structure thickness) alone could not differentiate between biofilm and mucus, due to their similar thickness metrics. We addressed this by deriving and extracting the optical attenuation coefficients of the biological materials from the OCT images.

In this study, we observed that the attenuation coefficient values decreased at some data points (days) for biofilm-positive ETTs (Figure 4A). This could be due to the standard-of-care suctioning which was performed approximately every 4-5 h, depending on patient needs, and may have been at a time immediately prior to OCT imaging, as we did not control for or alter the suctioning time intervals in this study. We hypothesize that the saline solution used for this procedure would likely coat the inner lumen of the ETT and any

associated biofilm, as well as possibly transiently change the optical properties of the biofilm, both of which would likely decrease the attenuation signal. Despite the use of regular standard-of-care suctioning, our results suggest that this procedure is unsuccessful at eliminating the ETT biofilms, since we continued to observe a subsequent shift in attenuation over time. Corroborating our hypothesis that routine suctioning is inefficient at clearing ETT biofilms, an investigation by Xiol *et al.* recently demonstrated that a novel closed suctioning method in a porcine model was more efficient at clearing the established biofilm, in contrast to the conventional method [39]. In a future study, we aim to use catheter-based 3-D OCT to examine changes in the formation of ETT biofilms and/or mucus deposits depending on different suctioning procedures and time intervals.

Despite the noted advantages, the present study has a few limitations. As OCT is sensitive to optical refractive index that is not bacterial species specific, it does not characterize bacterial species. However, consolidating catheter-based OCT with Raman spectroscopy may address this limitation, as Raman spectra can provide the biochemical properties of the bacteria and biofilms [40-42]. This study utilized a commercial catheter-based OCT system with commercial catheters originally designed for imaging human coronary arteries. The working distance of these catheters was shorter (approx. 5 mm) than what would be preferred for 3-D imaging of a larger diameter adult-sized ETT (approx. 8.5 mm), hence only a sector of the ETT could be imaged at each longitudinal position. OCT catheters designed for use in larger lumens, such as in the gastrointestinal tract, are commonly balloon-tipped catheters that can be inflated *in vivo* to center the OCT imaging optics [43]. These balloon-tipped catheters, however, would not be appropriate for imaging the human airway due to the restricted airflow when inflated. We are developing a catheter with an expandable and retractable scaffold-like mechanism that would center the OCT imaging optics within the lumen of the ETT and allow free airflow during mechanical ventilation.

In this study we used a commercial catheter OCT system (St. Jude Medical, Inc.) which only saved processed OCT amplitude data. Hence, a pixel-wise attenuation coefficient method was implemented. In the future, we will investigate and also incorporate *in vivo* viscosity measurements[44] to help differentiate between types of mucus and biofilms, or for any signs of debris that may be present. Furthermore, we will incorporate additional image processing techniques to identify biofilms that may vary depending on various respiratory co-morbidities such as chronic bronchitis, chronic obstructive pulmonary disease (COPD), or acute respiratory distress syndrome (ARDS). For example, a recent study showed the segmentation of an airway lumen and mucus based on mean backscattering intensity and grey level co-occurrence matrix statistics[45]. We will explore similar approaches to identify and differentiate biofilms and segment the image for attenuation coefficient analysis. Finally, image processing and display could be accelerated. The RAC data presented in the work were processed offline and required approximately 10 min per 3-D volume on a high-end desktop PC. In the future, we will implement a real-time attenuation coefficient processing and display algorithm on a GPU-based desktop computer that provides similar images rapidly at the point-of-care for prompt feedback to the physician for patient management decisions.

5 Conclusion

This investigation demonstrates a catheter-based 3-D OCT system for the longitudinal detection and monitoring of ETT biofilms in ventilated critical care patients. An optical attenuation-based analysis method was implemented to differentiate the observed biological structures between higher attenuating biofilms versus lesser attenuating mucus. This study provides new data and insights on the development of biofilms in ETTs, and suggests that OCT may be used to generate new image-based biomarkers for medical decision making in the management of ventilated critical care patients.

Supplementary Material

Refer to Web version on PubMed Central for supplementary material.

Acknowledgements

We acknowledge the logistical assistance from the research staff at Carle Foundation Hospital, and specifically thank Paula Bradley and Ashley Neef. This work was performed, in part, by utilizing the shared equipment and services of the Microscopy Suite and Visualization Laboratory at the Beckman Institute for Advanced Science and Technology at the University of Illinois at Urbana-Champaign (UIUC-BI-MS, UIUC-BI-VL). The authors thank Scott J. Robinson from the UIUC-BI-MS, for his assistance in operating the scanning electron microscope. Additional information can be found at http://biophotonics.illinois.edu

Funding

Research in this publication was supported in part by the National Institute for Biomedical Imaging and Bioengineering and the National Cancer Institute of the U.S. National Institutes of Health under award numbers R01EB013723 and R01CA213149, respectively. One hundred percent of the total project costs were financed with Federal money and zero percent of the total costs were financed by non-governmental sources. The content is solely responsibility of the authors and does not necessarily represent the official views of the National Institutes of Health.

References

[1]. Adair CG, Gorman SP, Feron BM, Byers LM, Jones DS, Goldsmith CE, Moore JE, Kerr JR, Curran MD, Hogg G Intensive Care Med. 1999, 25, 1072-1076. [PubMed: 10551961]

[2]. Diaz E, Rodríguez AH, Rello J Respir Care. 2005, 50, 900-909. [PubMed: 15972111]

[3]. Girou E, Schortgen F, Delclaux C, Brun-Buisson C, Blot F, Lefort Y, Lemaire F, Brochard L JAMA. 2000, 284, 2361-2367. [PubMed: 11066187]

[4]. Richards MJ, Edwards JR, Culver DH, Gaynes Crit RP. Care Med.1999, 27, 887-892.

[5]. Vincent J-L The Lancet. 2003, 361, 2068-2077.

[6]. Hunter JD Postgraduate medical journal. 2006, 82, 172-178. [PubMed: 16517798]

[7]. Rello J, Allegri C, Rodriguez A, Vidaur L, Sirgo G, Gomez F, Agbaht K, Pobo A, Diaz E The Journal of the American Society of Anesthesiologists. 2006, 105, 709-714.

[8]. Safdar N, Crnich CJ, Maki DG Respir Care. 2005, 50, 725-741. [PubMed: 15913465]

[9]. Rubenfeld GD, Caldwell E, Peabody E, Weaver J, Martin DP, Neff M, Stern EJ, Hudson LD New England Journal of Medicine. 2005, 353, 1685-1693. [PubMed: 16236739]

[10]. Park DR Respir Care. 2005, 50, 742-763; discussion 763-765. [PubMed: 15913466]

[11]. Augustyn B Crit Care Nurse. 2007, 27, 32-39. [PubMed: 17671243]

[12]. Jefferson KK FEMS Microbiol. Lett.2004, 236, 163-173. [PubMed: 15251193]

[13]. Bongiorni MG, Tascini C, Tagliaferri E, Cori AD, Soldati E, Leonildi A, Zucchelli G, Ciullo I, Menichetti F EP Europace. 2012, 14, 1334-1339.

[14]. Donlan RM Emerging infectious diseases. 2001, 7, 277-281. [PubMed: 11294723]

[15]. Tran PL, Lowry N, Campbell T, Reid TW, Webster DR, Tobin E, Aslani A, Mosley T, Dertien J, Colmer-Hamood JA, Hamood AN Antimicrobial agents and chemotherapy. 2012, 56, 972-978. [PubMed: 22123688]

[16]. Abidi SH, Sherwani SK, Siddiqui TR, Bashir A, Kazmi SUBMC Ophthalmology. 2013, 13, 57. [PubMed: 24134792]

[17]. Danin P-E, Girou E, Legrand P, Louis B, Fodil R, Christov C, Devaquet J, Isabey D, Brochard L Respir Care. 2015, 60, 21. [PubMed: 25371399]

[18]. Kalanuria AA, Zai W, Mirski M Crit Care. 2014, 18, 208. [PubMed: 25029020]

[19]. Kollef MH Am J Respir Crit Care Med. 2006, 173, 1182-1184. [PubMed: 16738261]

[20]. Torres A, Fàbregas N, Ewig S, de la Bellacasa JP, Bauer TT, Ramirez Crit J. Care Med.2000, 28, 2799-2804.

[21]. Wang G, Ji X, Xu Y, Xiang X Crit Care. 2016, 20.

[22]. Winer-Muram HT, Steiner RM, Gurney JW, Shah R, Jennings SG, Arheart KL, Eltorky MA, Meduri GU Radiology. 1998, 208, 193-199. [PubMed: 9646813]

[23]. Wunderink RG CHEST. 2000, 117, 188S-190S. [PubMed: 10816034]

[24]. Monroy GL, Hong W, Khampang P, Porter RG, Novak MA, Spillman DR, Barkalifa R, Chaney EJ, Kerschner JE, Boppart SA Otolaryngol Head Neck Surg. 2018, 194599818766320.

[25]. Monroy GL, Shelton RL, Nolan RM, Nguyen CT, Novak MA, Hill MC, McCormick DT, Boppart SA Laryngoscope. 2015, 125, E276-282. [PubMed: 25599652]

[26]. Nguyen CT, Jung W, Kim J, Chaney EJ, Novak M, Stewart CN, Boppart SA PNAS. 2012, 109, 9529-9534. [PubMed: 22645342]

[27]. Heidari AE, Moghaddam S, Truong KK, Chou L, Genberg C, Brenner M, Chen Z J Biomed Opt. 2015, 20, 126010. [PubMed: 26720877]

[28]. Sharma GK, Ahuja GS, Wiedmann M, Osann KE, Su E, Heidari AE, Jing JC, Qu Y, Lazarow F, Wang A, Chou L, Uy CC, Dhar V, Cleary JP, Pham N, Huoh K, Chen Z, Wong BJF Am J Respir Crit Care Med. 2015, 192, 1504-1513. [PubMed: 26214043]

[29]. Vermeer KA, Mo J, Weda JJA, Lemij HG, de JF Boer Biomedical Optics Express. 2013, 5, 322-337. [PubMed: 24466497]

[30]. Fahy JV, Dickey BF New England Journal of Medicine. 2010, 363, 2233-2247. [PubMed: 21121836]

[31]. Flemming H-C, Wingender J, Szewzyk U, Steinberg P, Rice SA, Kjelleberg S Nature Reviews Microbiology. 2016, 14, 563-575. [PubMed: 27510863]

[32]. Hotterbeekx A, Xavier BB, Bielen K, Lammens C, Moons P, Schepens T, Ieven M, Jorens PG, Goossens H, Kumar-Singh S, Malhotra-Kumar S Scientific Reports. 2016, 6, 36507. [PubMed: 27812037]

[33]. Gil-Perotin S, Ramirez P, Marti V, Sahuquillo JM, Gonzalez E, Calleja I, Menendez R, Bonastre J Crit Care. 2012, 16, R93. [PubMed: 22621676]

[34]. Adair C, Gorman S, Byers L, Jones D, Feron B, Crowe M, Webb H, McCarthy G, Milligan K Intensive Care Med. 2002, 28, 426-431. [PubMed: 11967596]

[35]. Pérez-Granda MJ, Latorre MC, Alonso B, Hortal J, Samaniego R, Bouza E, Guembe M BMC Infect Dis. 2017, 17.

[36]. Alkawareek MY, Algwari QT, Laverty G, Gorman SP, Graham WG, O'Connell D, Gilmore BF PLoS ONE. 2012, 7, e44289. [PubMed: 22952948]

[37]. Biel MA, Sievert C, Usacheva M, Teichert M, Wedell E, Loebel N, Rose A, Zimmermann R Lasers in Surgery and Medicine. 2011, 43, 586-590. [PubMed: 21987599]

[38]. Li H, Song C, Liu D, Ai Q, Yu J Int J Clin Exp Med. 2015, 8, 11075-11084. [PubMed: 26379907]

[39]. Aguilera Xiol E, Li Bassi G, Wyncoll D, Ntoumenopoulos G, Fernandez-Barat L, Marti JD, Comaru T, De Rosa F, Rigol M, Rinaudo M, Ferrer M, Torres A British Journal of Anaesthesia. 2015, 115, 775-783. [PubMed: 26475806]

[40]. Ayala OD, Wakeman CA, Pence IJ, O'Brien CM, Werkhaven JA, Skaar EP, Mahadevan-Jansen A Analytical Methods. 2017, 9, 1864-1871.

[41]. Kloß S, Kampe B, Sachse S, Rösch P, Straube E, Pfister W, Kiehntopf M, Popp J Anal. Chem. 2013, 85, 9610-9616. [PubMed: 24010860]

[42]. Zhao Y, Monroy GL, You S, Shelton RL, Nolan RM, Tu H, Chaney EJ, Boppart SA J Biomed Opt. 2016, 21, 107005. [PubMed: 27802456]

[43]. in NvisionVLE® Imaging System, Vol. (Ed.^Eds.: Editor), City.

[44]. Monroy GL, Pande P, Shelton RL, Nolan RM, Spillman DR, Porter RG, Novak MA, Boppart SA J Biophotonics. 2017, 10, 394-403. [PubMed: 27009636]

[45]. Adams DC, Pahlevaninezhad H, Szabari MV, Cho JL, Hamilos DL, Kesimer M, Boucher RC, Luster AD, Medoff BD, Suter MJ Biomedical Optics Express. 2017, 8, 4729-4741. [PubMed: 29082098]

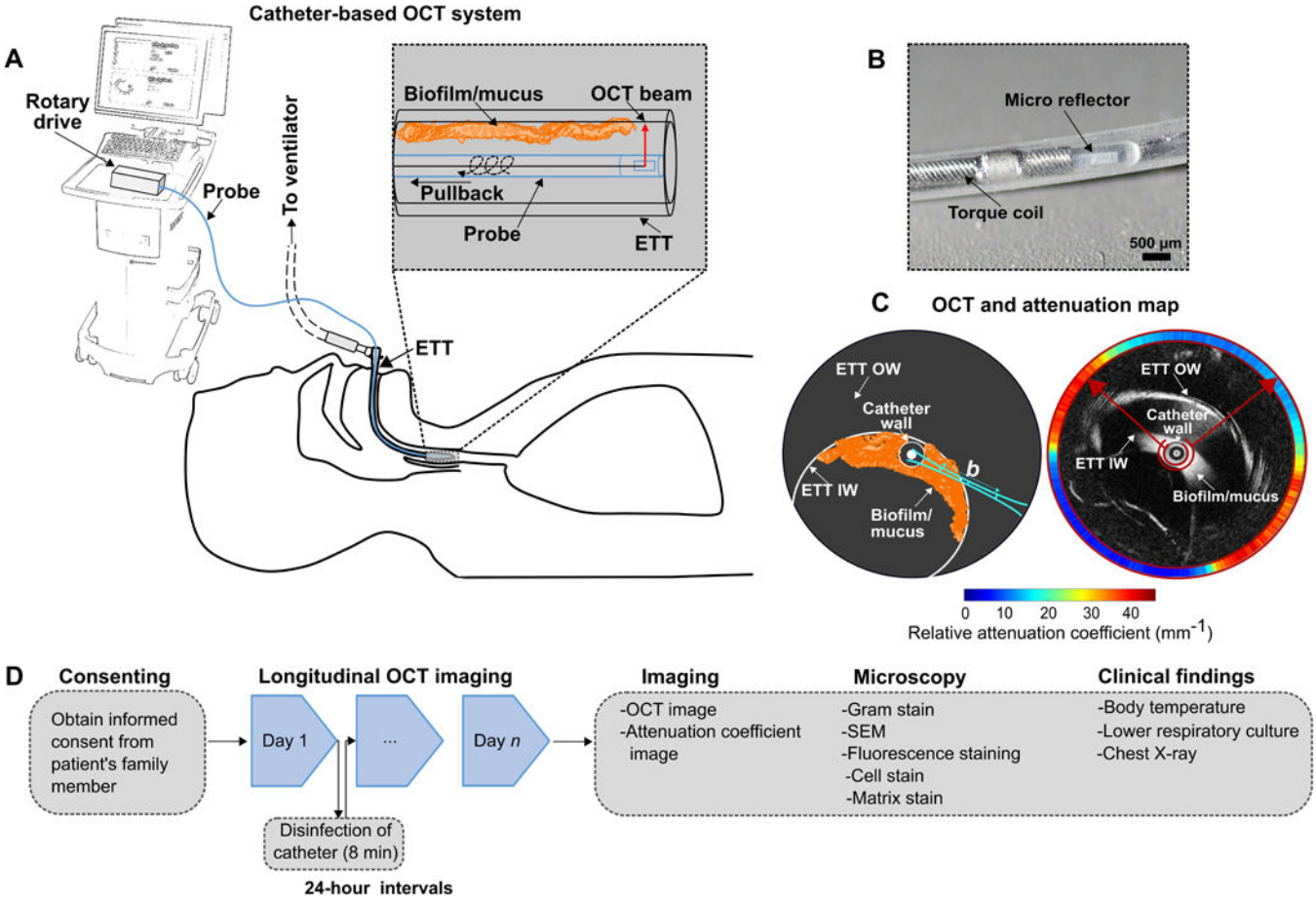

Figure 1.

Illustration of *in vivo* ETT imaging of intubated critical care patients using the catheter-based 3-D OCT system. (A) The OCT system used for imaging of biofilms or mucus in the ETT of the intubated subjects. (B) Magnified image showing the distal end and micro-optics of the OCT imaging catheter (Dragonfly C7). (C) Schematic illustration and representative OCT and attenuation coefficient image of an ETT. The OCT system will image the biofilm/mucus formed at the inner surface of the ETT. The approximate location of the OCT beam focus and confocal parameter or depth-of-field (b) is shown. An optical attenuation coefficient map was generated to differentiate between mucus and biofilm. The attenuation coefficient map corresponds to the mean attenuation coefficient values of the biofilm or mucus, measured from within the inner red ring shown overlaid with the OCT image, and further described in the Methods section. (D) Study flowchart. Following informed consent, imaging was performed to demonstrate the detection, formation, and differentiation of biofilm from mucus at 24 h intervals. OCT images were analyzed based on the differing optical attenuation coefficients. After extubation, ETT tubes were fixed and processed for conventional staining techniques and correlated with OCT images and clinical reports. ETT IW: ETT inner wall; ETT OW: ETT outer wall; *b*: depth-of-field.

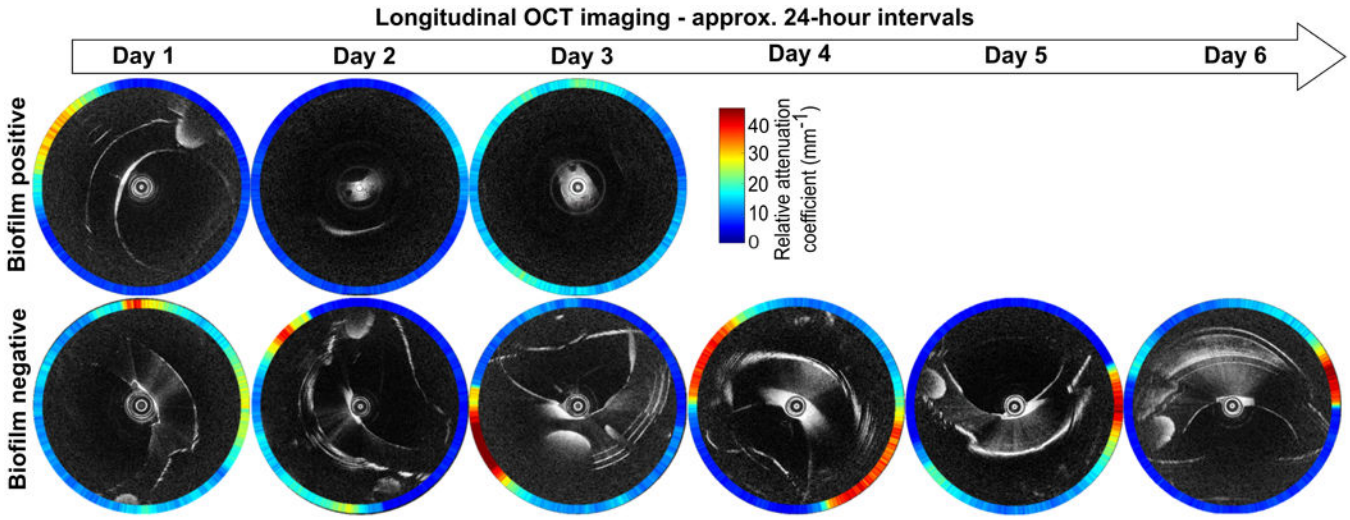

Figure 2.

Representative longitudinal *in vivo* OCT and RAC images from two intubated critical care subjects using the catheter-based OCT system. The top row shows representative longitudinal OCT images of an ETT without a biofilm present (Subject 6, extubated after 3 days). The bottom row shows representative longitudinal OCT images of an ETT with the presence and development of a biofilm (Subject 2, extubated after 6 days). Note that the RAC values are represented by a colored circumferential ring around each OCT image that corresponds to the radial RAC value through the biological material present around the catheter.

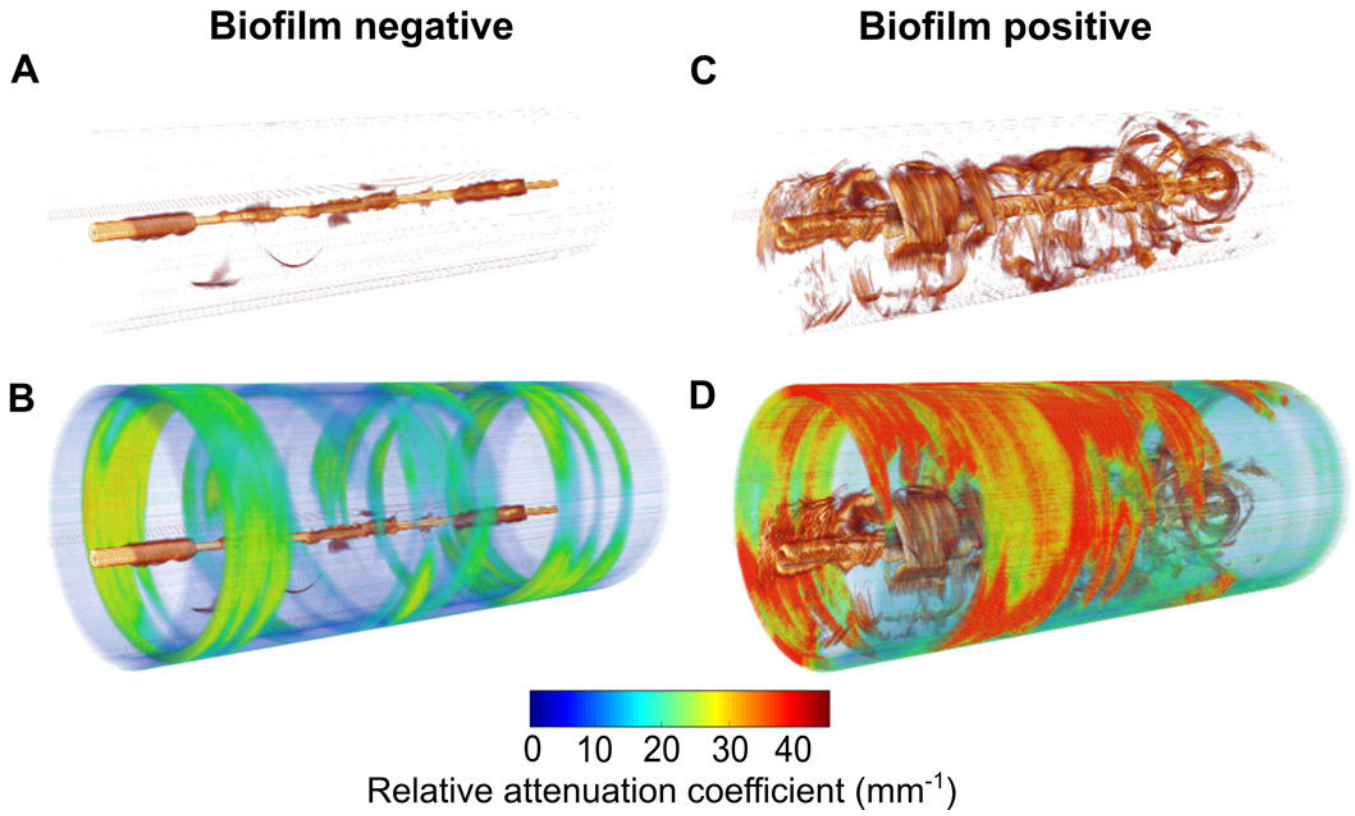

Figure 3.

Representative 3-D volume reconstructions of OCT and RAC images along the entire length of the ETT (straightened for visualization purposes). (A) 3-D OCT and (B) RAC images from an ETT that was negative for biofilm (Subject 6, Day 3). (C) 3-D OCT and (D) RAC images from an ETT positive for biofilm (Subject 2, Day 6). Increased optical attenuation from the biological structures within the ETT tube identifies the presence and 3-D distribution of biofilm throughout the length of the ETT.

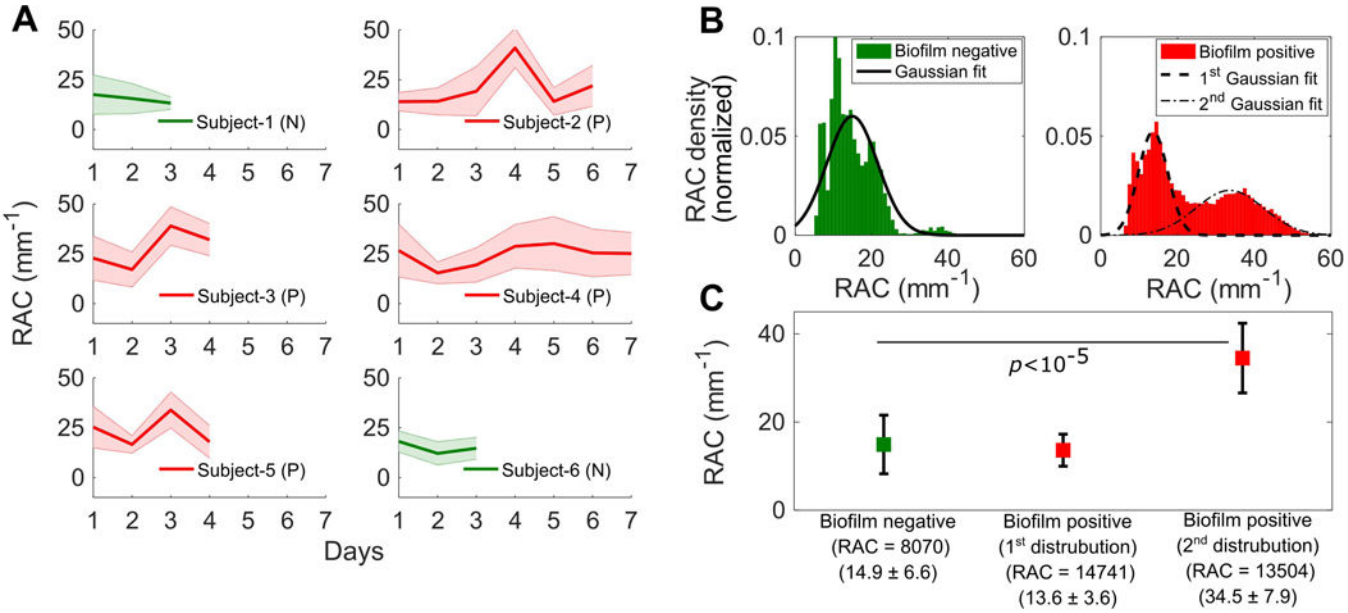

Figure 4.

Quantitative analysis of ETTs based on RAC metrics between groups. (A) Plots showing the mean RAC for all subjects (Subjects 1-6) from the day of intubation until extubation. The plots in green represent biofilm-negative (N) ETTs and plots in red represent biofilm-positive (P) ETTs. The lines represent the trends for the mean RAC values while the shaded regions represent the standard deviation of the RAC values. (B) Histogram plot and fit of all ETT RAC values. (C) Measured average RAC values, standard deviations, and statistical analysis presented by group.

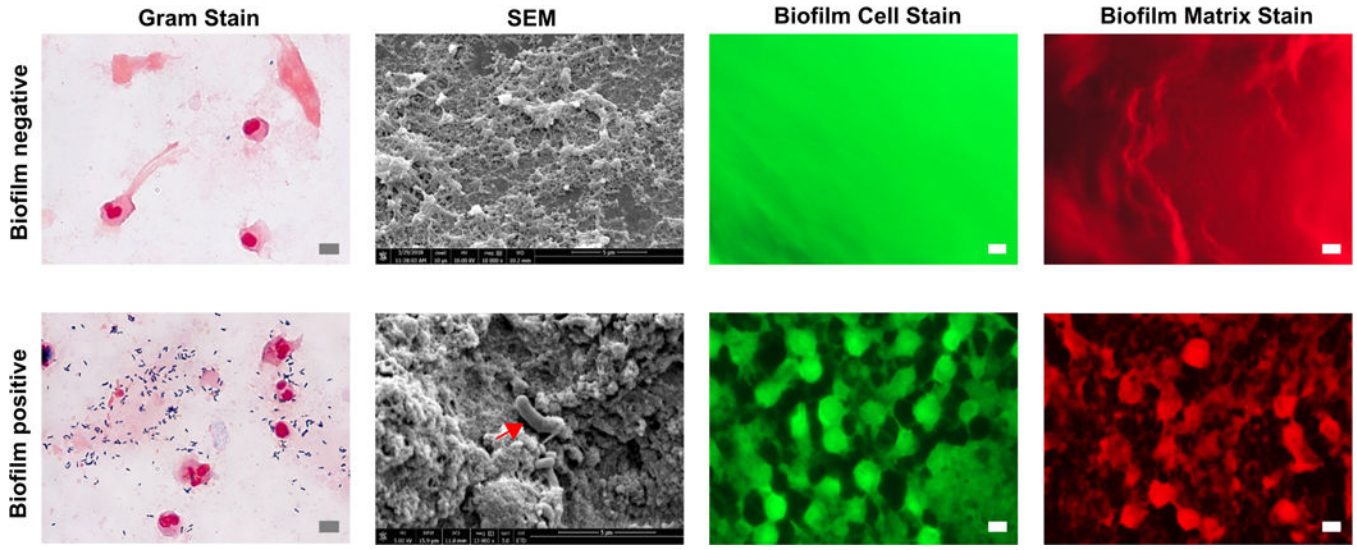

Figure 5.

Representative photomicrographs of biofilm-negative (top row) and biofilm-positive (bottom row) samples from ETTs. Gram stain of a paraffin-embedded biofilm-positive sample shows clusters of bacteria. SEM image shows the biofilm matrix along with embedded bacteria (red arrow). Bacterial cells and biofilm matrix appear when stained with FM-1-43 and SYPRO Ruby Red, confirming the presence of the ETT biofilm. Scale bars represent 5 μm.

Table 1.

Clinical findings of ventilated patients included in the study

Day	Body Temp (°C)	Age	Sex	Sputum screen	LRC	XR CHEST	
						Pleural effusion	Other notes
Subject - 1							
1	37.2	62	F	Rare SEC; Many PMNs	Rare amount *Candida albicans* recovered	No effusions	Persistent mild PVC; HL
2	36.9			--	--	No effusions	HL
3	36.6			--	--	--	--
Subject - 2							
1	37.8	69	M	Rare SEC; Many PMNs; Many gram positive cocci	Mixed upper respiratory flora recovered.	PE	ARF with hypoxia
2	37.4			--	--	Recurrent left PE	ARF with hypoxia; SE
3	36.9			--	--	Recurrent left PE	ARF with hypoxia; SE
4	36.4			--	--	Recurrent left PE	ARF with hypoxia; SE
5	37.6			--	--	Recurrent left PE	ARF with hypoxia; SE
6	37.3			--	--	Recurrent left PE	ARF with hypoxia; SE; Right lower lobe opacity; Pneumonia/pneumonitis; Left perihilar infiltrate
Subject - 3							
1	37.4	62	F	Rare SEC; Many PMNs	Mixed upper respiratory flora recovered.	Left PE	PE
2	37.1			--	--	Left PE	BPn
3	36.7			--	--	Left PE	AP; BPn
4	37.1			--	--	Left PE	Persistent BPI
Subject - 4							
1	37.7	44	F	--	--	--	ARF; High suspicion for pneumonia
2	37.6			PMNs	--	--	ARF; High suspicion for pneumonia
3	37.2			--	--	--	ARF; High suspicion for pneumonia
4	36.9			--	--	--	ARF; High suspicion for pneumonia
5	36.3			--	--	--	ARF; Probably VAP
6	36.9			--	--	--	ARF; Probably VAP
7	39			--	--	--	ARF; Pneumonia - staph aureus
Subject - 5							
1	37.2	52	F	Rare amount of *Candida albicans* recovered	--	--	ARF; AP (possible pneumonia)
2	36.5			--	--	--	ARF; AP (possible pneumonia)
3	36.8			--	--	--	ARF; AP (possible pneumonia)

Day	Body Temp (°C)	Age	Sex	Sputum screen	LRC	XR CHEST	
						Pleural effusion	Other notes
4	38.1			Rare SEC; Many PMNs; Rare gram - bacilli	Moderate amount of *Pseudomonas aeruginosa* recovered	--	ARF; AP (possible pneumonia)
Subject - 6							
1	37.6	72	F	Rare SEC; Many PMNs;	--	--	ARF; Left sided pneumothorax
2	36.6	--	--	--	ARF; Left sided pneumothorax		
3	37.3	--	--	--	ARF; Left sided pneumothorax		

LRC, Lower respiratory culture; *SEC,* Squamous epithelial cells; *PMN,* Polymorphonuclear leukocytes; *PE,* Pleural effusion; *ARF,* Acute respiratory failure; *SE,* Subcutaneous emphysema; *BPI,* Bilateral pulmonary infiltrates; *BPn,* Bilateral pneumonitis; *PE,* Pulmonary edema; *AP,* Aspisration pneumonia; *PVC,* Pulmonary vascular congestion; *HL,* Hyperinflated lungs; *VAP,* Ventilator-associated pneumonia; -- indicates data unavailable